J. Fluid Mech. (2007), *vol.* 575, *pp.* 27–55.
doi:10.1017/S0022112006003752 Printed in the United Kingdom

Nonlinear reflection of grazing acoustic shock waves: unsteady transition from von Neumann to Mach to Snell–Descartes reflections

SAMBANDAM BASKAR, FRANÇOIS COULOUVRAT† AND RÉGIS MARCHIANO

Laboratoire de Modélisation en Mécanique, Université Pierre et Marie Curie–Paris 6 & CNRS (UMR 7607), 4 place Jussieu, 75252 Paris cedex 05, France

(Received 9 December 2005 and in revised form 31 August 2006)

We study the reflection of acoustic shock waves grazing at a small angle over a rigid surface. Depending on the incidence angle and the Mach number, the reflection patterns are mainly categorized into two types, namely regular reflection and irregular reflection. In the present work, using the nonlinear KZ equation, this reflection problem is investigated for extremely weak shocks as encountered in acoustics. A critical parameter, defined as the ratio of the sine of the incidence angle and the square root of the acoustic Mach number, is introduced in a natural way. For step shocks, we recover the self-similar (pseudo-steady) nature of the reflection, which is well known from von Neumann's work. Four types of reflection as a function of the critical parameter can be categorized. Thus, we describe the continuous but nonlinear and non-monotonic transition from linear reflection (according to the Snell–Descartes laws) to the weak von-Neumann-type reflection observed for almost perfectly grazing incidence. This last regime is a new, one-shock regime, in contrast with the other, already known, two-shock (regular reflection) or three-shock (von Neumann-type reflection) regimes. Hence, the transition also resolves another paradox on acoustic shock waves addressed by von Neumann in his classical paper. However, step shocks are quite unrealistic in acoustics. Therefore, we investigate the generalization of this transition for N-waves or periodic sawtooth waves, which are more appropriate for acoustics. Our results show an unsteady reflection effect necessarily associated with the energy decay of the incident wave. This effect is the counterpart of step-shock propagation over a concave surface. For a given value of the critical parameter, all the patterns categorized for the step shock may successively appear when the shock is propagating along the surface, starting from weak von-Neumann-type reflection, then gradually turning to von Neumann reflection and finally evolving into nonlinear regular reflection. This last one will asymptotically result in linear regular reflection (Snell–Descartes). The transition back to regular reflection is one of two types, depending on whether a secondary reflected shock is observed. The latter case, here described for the first time, appears to be related to the non-constant state behind the incident shock, which prevents secondary reflection.

† Author to whom correspondence should be addressed: coulouvr@ccr.jussieu.fr

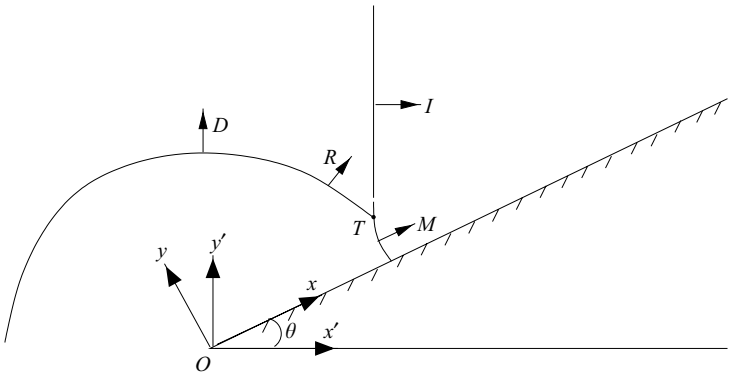

FIGURE 1. Reflection of a grazing wave: the geometry of the physical problem. I, incident shock; R, reflected shock; T, triple point; M, Mach shock; and D, diffracted shock.

1. Introduction

As soon as a plane shock wave of acoustic Mach number M_a impinges on a rigid inclined surface with a grazing angle θ $(0 < \theta < \pi/2)$, it gives rise to a reflected shock. The incident and reflected shocks, as they propagate (for instance, from left to right as shown in figure 1) along the rigid surface, result in a reflection pattern which can be basically of two types, namely regular and irregular reflections (see Ben-Dor 1992). The type of reflection depends on the grazing angle and the strength of the incident shock. For a sufficiently large angle, or a sufficiently weak shock, the incident and the reflected shocks intersect right at the rigid surface. This type of reflection is called regular reflection.

As the angle decreases, or the shock amplitude increases, the point of intersection T of the incident and reflected shocks detaches from the surface. Owing to the nonlinear interaction of these two shocks at T, a new shock emerges to ensure contact with the surface. This emerging shock is called a Mach shock or Mach stem, and the point T of intersection of these three shocks is called the triple point. This type of reflection is known as *irregular reflection.*

For a strong incident shock, in addition to these three shocks at T, there exists also a contact discontinuity (the slipstream). It divides the flow behind the reflected and the Mach shock into two states across which the normal velocity component and the pressure are continuous, whereas other quantities (tangential velocity, density, temperature, entropy) undergo a jump discontinuity. This is known as Mach reflection and is named after its first experimental observation by Mach (1878). This famous work of Mach has given birth to a new field of research commonly known as shock-wave reflection phenomena (see Ben-Dor & Takayama 1992).

Theoretical investigation of shock-wave reflection was first carried out by von Neumann (1943) for inviscid perfect gases. His theory on irregular reflection is called three-shock theory, while two-shock theory refers to regular reflection. Criteria for the transition between the two types of reflection are derived from these theories (see Henderson 1987). A basic assumption made in the derivation of these theories is the pseudo-steady (or self-similar) nature of the flow. These theories also assume that all the waves in the flow are either shocks with negligible curvature separating constant states or contact discontinuities with negligible thickness (a slipstream).

The three-shock theory has good agreement with experiment near the transition criteria when the incident shock Mach number is greater than 1.47, which is considered

to be a strong shock (see Colella & Henderson 1990). For weak shocks (with incident shock Mach number less than 1.035) the three-shock theory leads to the conclusion that the Mach reflection is physically unrealistic, while experimental evidence supported by numerical simulations (from inviscid Euler equations) shows that Mach reflection still remains possible for such weak shocks (see Colella & Henderson 1990). The discrepancy between the three-shock theory and the experimental studies has been referred to as the *von Neumann paradox*. It was first stated by Birkhoff (1950) and later more precisely by Colella & Henderson (1990). Several attempts have been made to resolve this paradox either experimentally or theoretically, with different proposed explanations. This nevertheless remains a challenging open problem.

For the case where the three-shock theory gives unrealistic results, Colella & Henderson (1990) observed numerically and experimentally a continuous slope of the shock front along the incident and the Mach shock. Their numerical results show that this continuous slope occurs because the reflected shock breaks down into a band of compressive waves as it approaches the incident shock and so there is no triple point. They named this new type of reflection the *von Neumann reflection*, which they introduced as a different regime from Mach reflection (where the slope has a discontinuity at the triple point, as described by three-shock theory). Henderson, Crutchfield & Virgona (1997) provided computational and experimental evidence of the importance of viscosity and heat conductivity in the flow in solving the paradox. The boundary condition on the slipstream separating the two constant states behind the triple point has been questioned by Skews (1972) (see also Ben-Dor 1987; Kobayashi, Adachi & Suzuki 1995), and recently Kobayashi, Adachi & Suzuki (2004) gave experimental evidence for the non-self-similar nature of weak Mach reflection. A singularity in the reflected shock curvature at the triple point, shown by Sternberg (1959), or a singularity in the solution behind the triple point, shown by Tabak & Rosales (1994), are other proposed explanations of the paradox. For more details on the literature of the paradox and also a detailed discussion of all possible types of reflection with their transition criteria, we refer to the review article by Ben-Dor & Takayama (1992). Hunter & Brio (2000) studied weak shock reflection in the case of step shocks using the two-dimensional Burgers' equation. This enabled them to capture a very tiny supersonic patch behind the triple point, which was initially hypothesized by Guderley (1962). They also proved theoretically the existence of an expansion fan at the triple point in addition to the three shocks, which is yet another explanation for the paradox. Such a reflection pattern was also first proposed by Guderley (1962) and is commonly known as *Guderley reflection*. From different numerical solvers of the Euler equations, Vasil'ev & Kraiko (1999) and Zakharian *et al.* (2000), respectively, captured the expansion fan and the supersonic patch. Tesdall & Hunter (2002) investigated the problem further and found (through a new numerical scheme developed by them) a more complex structure of the reflection pattern with a sequence of triple points along the Mach shock, each one associated with an additional expansion fan. This whole complex structure takes place very locally in a tiny domain behind the leading triple point. Recently, Skews & Ashworth (2005) performed a very-high-resolution experiment which gave evidence of the presence of a multireflection structure behind the three-shock reflection.

Extremely weak shock waves do exist in the acoustic regime corresponding to Mach numbers not much larger than 1.001 (while for instance the experiments of Colella & Henderson (1990) do not go below Mach 1.035 and those of Skews & Ashworth (2005) do not go below Mach 1.04). Examples of such shock waves are sonic booms in the

atmosphere at the ground level and ultrasonic shock waves produced by piezoelectric arrays in water for high-frequency ultrasound therapy (such as lithotripsy). The objective of the present study is to investigate the nonlinear reflection of acoustic shock waves and to determine whether the reflection of extremely weak acoustic shock waves is specific. With this viewpoint several unanswered questions must be addressed. The first concerns the different regimes of reflection of acoustic weak shock waves depending on the shock amplitude and the incidence angle. Though acoustic shock waves are extremely weak, they are nonetheless intrinsically nonlinear. However it remains uncertain whether nonlinear effects play a role at some stage during the reflection or whether, on the contrary, acoustic shock waves still satisfy the linear Snell–Descartes laws of reflection. Indeed, von Neumann (1943) hypothesized that acoustic shock waves behave differently from stronger shocks. The question is therefore to match the linear Snell–Descartes laws with weak-shock theory. Another open question was pointed out by von Neumann (1943), who remarked that the linear Snell–Descartes laws are themselves singular. Indeed, they predict the well-known pressure doubling at the reflector surface, which is valid (in the linear theory) for any grazing angle except the perfectly grazing angle. For the perfectly grazing case, the incident shock wave propagates exactly parallel to the surface, there is no reflection at all and no pressure doubling. Therefore, even in the linear regime the Snell–Descartes laws are singular, another paradox that we suggest should be called the acoustic von Neumann paradox. In his original paper, von Neumann conjectures that for acoustic waves there is a smooth and monotonic transition between the Snell–Descartes laws and perfectly grazing incidence, in contrast with the strong-shock case. The first main objective of the present study is therefore to investigate this transition systematically.

Another key feature of acoustic shock waves is that they are never the perfect step shock between constant states that has been solely examined in the above-cited studies. Indeed, acoustic shock waves are always preceded or followed by non-constant flows which modify the reflection structure. Also, acoustic shock waves are frequently not unique but appear as a sequence of two or more shocks. For instance, a sonic boom typically has the shape of an N-wave (two shocks) while long trains of ultrasound have the shape of a periodic sawtooth wave. In all these cases, we expect the multiple incident and reflected shock waves to interact with one another. Our second main objective here is therefore to examine whether the categorization of the shock-reflection regimes that applies for a the step shock remains valid for other kinds of acoustic shock waves.

In the case of a weak shock incident on a reflector at a small grazing angle, the wave propagation (whose direction is given by the normal to the wavefront as shown in figure 1) is mostly oriented parallel to the reflecting surface. As the direction of propagation of the reflected wave will also deviate only slightly from the tangent to the reflector, this suggests that instead of the two-dimensional Euler equations, the KZ equation (see Zabolotskaya & Khokhlov 1969) may be used with effect (§ 2). Indeed, the KZ equation is derived under two main assumptions: weak shocks and propagation in a preferred direction. Both are obviously well satisfied here, which makes the use of this equation especially well suited to the present case. Note that this equation is equivalent to the two-dimensional Burgers' equation used by Hunter & Brio (2000). In the derivation of the boundary conditions for the KZ equation, a critical parameter a is introduced naturally (§ 3), which shows that the acoustic-shock strength has to be of the order of the square of the grazing angle θ for full coupling between nonlinear and diffraction effects near the surface; a similar kind of parameter

was introduced by Hunter & Brio (2000). Then a self-similar rule is obtained for the step shock in the acoustic regime. The self-similar rule is verified numerically in § 4. We also show that, unlike nonlinear Fresnel diffraction (see Coulouvrat & Marchiano 2003), the flow for the N-wave or the periodic sawtooth wave does not follow any self-similar law.

We then derive in § 5 a transition condition from regular to irregular reflection for a step shock; this is a general form of the detachment condition derived by Hunter (1991). By varying the critical parameter a, we study the different types of reflection, starting from linear regular reflection for a very large value of a (Snell–Descartes reflection) to the so-called weak von Neumann reflection for a small value of a, in which we observe a smooth reflected wave instead of a reflected shock. For intermediate values we recover the other regimes of reflection already found in the literature, as described above. Such a complete 'panorama' of step-shock reflection is the first main original result of this study and will enable us to solve the acoustic von Neumann paradox. The second main result is given by a numerical study of unsteady reflection phenomena in the case of N-waves and sawtooth waves (§ 6). In both cases we obtain new results, which are not possible for step shocks grazing over a plane rigid surface because step shock reflection is self-similar. In particular, we observe a non-monotonic trajectory for the triple point. This leads to intricate reflection patterns such as inverse Mach reflection and transitioned regular reflection of two types, one of which is described here for the first time. This type-2 reflection has a behaviour similar to the unsteady reflection discussed in Chapter 4 of Ben-Dor (1992) for step shocks grazing over a concave double wedge, but to our knowledge this behaviour is newly observed for the reflection of complex shock waveforms over a perfectly plane surface. Finally, we discuss unsteady effects related to the decrease in energy of the incident shock wave along the reflecting plate. This unsteadiness will be shown to imply continuous transition from the initial nonlinear shock-reflection regime at the tip of the plate up to the final linear Snell–Descartes reflection.

2. Shock-wave reflection and the KZ equation

We consider a two-dimensional plane shock wave grazing over a plane rigid surface with acoustic Mach number M_a (defined as the ratio of the maximum amplitude of the acoustic velocity over V_0, which is the excess of the wave velocity over the constant sound velocity c_0 in the undisturbed medium, and the ambient sound speed). Typical values of this Mach number are about 10^{-3} for observed sonic booms (of Concorde) or ultrasonic shock waves. Note this corresponds in the usual definition of the Mach number to values smaller than 1.001, much closer to 1 than the cases investigated previously in the literature (as mentioned in the introduction). The shock encounters a wedge of angle θ at point O as shown in figure 1. We assume a homogeneous and inviscid fluid of ambient density ρ_0. Let us take the longitudinal coordinate (normal to the incident wavefront) and the transverse coordinate (parallel to the incident wavefront) as x' and y' respectively. We denote the physical time by t and the oblique coordinates by x and y (respectively parallel and perpendicular to the reflecting surface) and fix the origin O at the tip of the wedge.

We define the dimensionless retarded time as $\tau' = \omega(t - x'/c_0)$, where ω is a reference angular frequency characteristic of the incident signal's duration or periodicity. We make the transverse and the longitudinal coordinates dimensionless by $Y' = y'/L$, $X' = x'/D$, where $L = 1/(k\sqrt{2\beta M_a})$ is the transverse length scale and $D = 1/(\beta k M_a)$ is the shock-formation distance; here $k = \omega/c_0$ is the wave number and $\beta = 1 +$

$B/2A$, B/A being the nonlinearity parameter (see Hamilton & Blackstock 1998). The dimensionless oblique coordinates and retarded time are defined similarly as $X = x/D$, $Y = y/L$ and $\tau = \omega(t - x/c_0)$.

We assume that (i) the grazing angle is small, $\theta \ll 1$ (the grazing-wave assumption), and (ii) the shock wave is weak, $M_a \ll 1$, which is appropriate for the acoustic case. These two assumptions justify the use of the paraxial approximation of the nonlinear wave equation, which is the well-known KZ equation (see Zabolotskaya & Khokhlov 1969),

$$\frac{\partial^2 P}{\partial X \partial \tau} - \frac{\partial^2 P}{\partial Y^2} = \frac{\partial^2}{\partial \tau^2}\left(\frac{P^2}{2}\right), \tag{2.1}$$

where $P = p_a/(\rho_0 c_0 V_0)$ is the dimensionless acoustic pressure with p_a the acoustic pressure. We recall that the KZ equation is an approximation of the Euler equations valid for finite-amplitude sound waves provided that two main assumptions are satisfied. The first requires waves of small amplitude; it is perfectly satisfied here for acoustic shocks because of the small value of the acoustic Mach number M_a. The second is the paraxial approximation, which assumes that waves propagate mainly into a preferred direction, here the direction tangent to the reflector surface. In its linearized form, the dispersion relation of the KZ equation replaces the exact dispersion relation of the wave equation, which is a circle, by the parabola tangent to this circle at the main direction of propagation. This justifies the name 'parabolic approximation', which is frequently used instead of 'paraxial approximation'. This approximation is estimated to be valid for directions of wave propagation that deviate from less than $\pm 30^\circ$, for which case the error in the dispersion equation is less than 1%. Here, we will study grazing angles for which the critical parameter introduced in the next section is typically less than 3, which corresponds to angles less than 8.5° in air and 14.5° in water, well within the range of validity of the paraxial approximation.

The KZ equation can be expressed in the form of two conservation equations,

$$\frac{\partial P}{\partial X} = \frac{\partial U}{\partial Y} + \frac{\partial}{\partial \tau}\left(\frac{P^2}{2}\right), \tag{2.2}$$

$$0 = \frac{\partial P}{\partial Y} - \frac{\partial U}{\partial \tau}, \tag{2.3}$$

which can also be viewed as the weak-disturbance asymptotic limit of the unsteady transonic problem (see Hunter 1991). Equation (2.2) is the well-known two-dimensional Burgers' equation, which takes care of the nonlinear effect; (2.3) includes the diffraction effect. Note however that, when compared with the two-dimensional Burgers' equation, the role of time and space have been interchanged in the KZ equation, which takes the form of an evolution equation in space rather than in time. This interchange is allowed by the equivalence between time and space through the introduction of the retarded time as the 'fast' variable in the multiple-scale asymptotic process sustaining the derivation of the KZ equation. An equivalent form but with evolution in time is known as the nonlinear progressive wave equation (NPE) equation (see McDonald & Kuperman 1987) and is strictly equivalent to the two-dimensional Burgers' equation discussed by Hunter (1991). Note also that, because of this interchange between time and space, the computed solutions appear as a succession of views in the (τ, Y)-plane with increasing X distances, instead of the more usual views in the (X, Y)-plane with increasing times. Visually, in figures 3, 6–8, 11, 12, 14 and 16, this makes the incident field inclined towards the left, as it arrives

earlier at positions more distant from the reflector surface. Similarly, the reflected field is inclined towards the right. To recover the usual viewpoint, as seen in figure 1, a horizontal reflection of the above listed figures is simply to be performed.

The Rankine–Hugoniot condition for the system (2.2), (2.3) is given by (see Coulouvrat & Marchiano 2003)

$$-W[P] = [U]N_Y + [P^2/2]N_\tau, \tag{2.4}$$

$$0 = [P]N_Y - [U]N_\tau, \tag{2.5}$$

where $[f] = f_2 - f_1$ is the notation for the jump in value of any quantity f across the shock, W is the shock-normal speed and $\boldsymbol{N} = (N_\tau, N_Y)$ is the normal vector to the shock wave $\tau_s = \tau_s(X, Y)$, which is a curve in (τ, Y)-space evolving with the propagation variable X. Eliminating U from the above two jump relations, we get the shock condition as

$$-WN_\tau = N_Y^2 + \langle P\rangle N_\tau^2, \tag{2.6}$$

where $\langle P\rangle = (P_1 + P_2)/2$ is the mean value of P. The shock-jump relations (2.4), (2.5) and their alternate form (2.6) are used in finding the transition condition from regular to irregular reflection derived in § 5.1. We use the KZ equation (2.1) to obtain numerical results for the shock-reflection problem in the (τ, Y)-plane for a given X. This numerical problem needs appropriate initial and boundary conditions, which will be examined in the next section.

3. The critical parameter and the boundary conditions

For computational purposes, it is convenient to work in the oblique coordinate system x, y, in which x and y are parallel and perpendicular to the wedge surface respectively, as shown in figure 1. We denote the corresponding non-dimensional coordinates as X, Y and the corresponding retarded time as τ, as already mentioned in § 2.

The relation between the coordinates X, Y and X', Y' is given by

$$X' = X\cos\theta - \frac{L}{D}Y\sin\theta = X + O(\sin^2\theta), \tag{3.1}$$

where L and D are defined in § 2. Here we make the fundamental assumption that $\theta = O(\sqrt{M_a})$. For typical acoustic Mach numbers of order 10^{-3}, this corresponds to grazing angles of the order of a few degrees. The transformation $Y' \to Y$ can be defined similarly, but it is not used anywhere in our problem. The relation between the retarded times τ' and τ is given by

$$\tau' = \tau + aY + a^2X + O(\sin^2\theta), \tag{3.2}$$

where the critical parameter a is naturally introduced as

$$a = \frac{\sin\theta}{\sqrt{2\beta M_a}} = O(1). \tag{3.3}$$

For numerical simulation we have to prescribe the incoming wave at $X = 0$, from which we get the initial pressure field in the (τ, Y)-plane for the computation. This incoming field is the solution of the one-dimensional Burgers' equation

$$\frac{\partial P}{\partial X'} - P\frac{\partial P}{\partial \tau'} = 0 \tag{3.4}$$

describing the propagation of a nonlinear plane wave in the X'-direction.

In our problem, we study three types of waves, namely the step shock, the N-wave and the sawtooth wave. We give the solution of the Burgers' equation in the (X', τ', Y')-variables for these three cases and then transfer the solution to the (X, τ, Y)-variables using the transformations (3.1)–(3.3).

(i) Step shock The solution of the incoming field in the (X', τ', Y')-variables is given by

$$P(X', \tau', Y') = \begin{cases} 0 & \text{if } \tau' \leqslant -X'/2, \\ 1 & \text{if } \tau' > -X'/2, \end{cases} \tag{3.5}$$

and the solution of the incoming field in the X, τ, Y variables is given by

$$P(X, \tau, Y) = \begin{cases} 0 & \text{if } \tau + aY + a^2X \leqslant -X/2, \\ 1 & \text{if } \tau + aY + a^2X > -X/2. \end{cases} \tag{3.6}$$

(ii) N-wave The solution of the incoming field in the (X', τ', Y')-variables is given by

$$P(X', \tau', Y') = \begin{cases} -\dfrac{\tau'}{X'+1} & \text{if } |\tau'| \leqslant \sqrt{(1+X')/2}, \\ 0 & \text{otherwise}, \end{cases} \tag{3.7}$$

and the solution of the incoming field in the (X, τ, Y)-variables is given by

$$P(X, \tau, Y) = \begin{cases} -\dfrac{\tau + aY + a^2X}{X+1} & \text{if } |\tau + aY + a^2X| \leqslant \sqrt{(1+X)/2}, \\ 0 & \text{otherwise}. \end{cases} \tag{3.8}$$

(iii) Periodic sawtooth wave The solution of the incoming field in the (X', τ', Y')-variables for each period in $[-1, 1]$ is given by

$$P(X', \tau', Y') = \begin{cases} -\dfrac{\tau'+1}{X'+1} & \text{if } -1 < \tau' \leqslant 0, \\ -\dfrac{\tau'-1}{X'+1} & \text{if } 0 < \tau' \leqslant 1, \end{cases} \tag{3.9}$$

and the solution of the incoming field in the (X, τ, Y)-variables for each period in $[-1, 1]$ is given by

$$P(X, \tau, Y) = \begin{cases} -\dfrac{(\tau + aY + a^2X + 1)}{X+1} & \text{if } -1 < \tau + aY + a^2X \leqslant 0, \\ -\dfrac{(\tau + aY + a^2X - 1)}{X+1} & \text{if } 0 < \tau + aY + a^2X \leqslant 1. \end{cases} \tag{3.10}$$

We note that the above wave is of period 2 with shocks at $0, \pm 2, \pm 4, \ldots$.

We denote the computational boundary in the (τ, Y)-variables as EFGH (see figure 2). We impose the rigid boundary condition $\partial P/\partial Y = 0$ on the boundary EF. Since the propagation of the shock wave is downstream, we use a backward difference for the τ variable in our finite-difference scheme, which makes the boundary FG a free boundary. This allows us to minimize the complications defining the condition on the boundary GH if we choose its length large enough that the reflected shock does not touch the boundary GH throughout the computation, as shown in figure 2. For the transient step shock and N-wave, we further assume that the incident shock

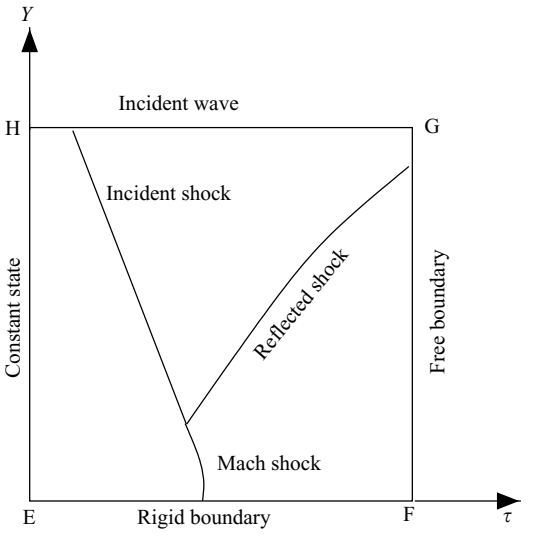

FIGURE 2. The computational domain and the boundary conditions.

enters the computational domain through the boundary GH, as shown in figure 2. With the above two assumptions, we can impose the solution ((3.6) or (3.8)) of the one-dimensional Burgers' equation (3.4) on the boundary GH and a constant state (zero) on the boundary HE. For a periodic sawtooth wave, the first assumption only is sufficient to impose the solution (3.10) of the one-dimensional Burgers' equation (3.4) on the boundary GH, while boundaries FG and HE are handled simultaneously by the periodicity condition. The numerical algorithm used to solve the KZ equation (2.1) in the transient case is identical to the split-step finite-difference scheme developed by Coulouvrat & Marchiano (2003) and Marchiano, Coulouvrat & Thomas (2005) to study the nonlinear diffraction of weak shock waves respectively by a screen or at a cusped caustic. The nonlinear part of the wave evolution is treated by a shock-fitting algorithm based on the exact Poisson solution and weak-shock theory, so as to minimize numerical dissipation and dispersion effects and track shock waves with highest precision. The linear diffraction part is solved by the finite-difference algorithm of Lee & Hamilton (1995). For the periodic case, the numerical solver is similar to that developed by Auger & Coulouvrat (2002) and Marchiano, Coulouvrat & Grenon (2003), where time derivatives for the diffraction part are evaluated by a pseudo-spectral technique to guarantee periodicity. The reader is referred to these publications for details about the scheme, including many validation tests such as the convergence of the solution with mesh refinement, comparison with analytical solutions or experimental data, or the recovery of self-similar properties of solutions. Here similar tests have been performed for the case of reflection with similar results, and therefore they are not all reproduced. However, self-similarity properties of the numerical solutions in agreement with the theory are demonstrated in the next section (see figure 3), and perfect agreement between the numerical simulations and two-shock theory in the case of nonlinear regular reflection is also demonstrated, later on (see figure 10). Finally, a preliminary comparison with experimental data also shows excellent agreement with the numerical simulations (see Baskar, Coulouvrat & Marchiano 2006).

4. About self-similarity

In this section, we discuss the similarity behaviour for the step-shock, N-wave and sawtooth wave reflection as a solution of the KZ equation. Self-similarity (also called pseudo-steadiness) of the step-shock reflection problem on a flat rigid surface has been assumed since the pioneering work of von Neumann (1943), and in most of the subsequent theoretical works mentioned in the introduction. First we will recover the self-similarity of the step-shock problem for the KZ equation, as expected from the work of Hunter & Brio (2000) using the equivalent two-dimensional Burgers' equation. However, we will show that this behaviour is restricted to the ideal case, while realistic acoustic signals such as N-waves or sawtooth waves will prove to be non-self-similar. In this case, we expect (as will be demonstrated in § 6) more complex nonlinear reflection effects similar to the unsteady reflection of a step shock over a concave double wedge (see Ben-Dor 1992). Notice that this case is different from the nonlinear Fresnel diffraction of weak shock waves, where all three kinds of wave exhibit self-similar behaviour (see Coulouvrat & Marchiano 2003).

We introduce the rescaling

$$P \to P^* P, \qquad X \to X^* X, \qquad Y \to Y^* Y \qquad \text{and} \qquad \tau \to \tau^* \tau, \tag{4.1}$$

where the asterisked quantities denote the rescaling amplitude of the corresponding variable.

The condition for the KZ equation (2.1) to be invariant under the above rescaling is given by

$$P^* = \tau^* / X^*, \qquad Y^* = \sqrt{X^* \tau^*}. \tag{4.2}$$

To make the step shock (3.6) invariant, we need to choose

$$P^* = 1, \qquad \tau^* = X^*, \qquad Y^* = X^*.$$

Hence, the self-similar solution for the step shock takes the form

$$P(X, \tau, Y) = Q\left(\xi = \frac{\tau}{X},\ \eta = \frac{Y}{X}\right). \tag{4.3}$$

Substituting the above self-similar solution into the KZ equation (2.1), we get

$$\frac{\partial Q}{\partial \xi} + \xi \frac{\partial^2 Q}{\partial \xi^2} + \eta \frac{\partial^2 Q}{\partial \eta \partial \xi} + \frac{\partial^2 Q}{\partial \eta^2} + \frac{1}{2} \frac{\partial^2 Q^2}{\partial \xi^2} = 0.$$

Obviously, the incident plane-wave equation (3.5) also satisfies self-similarity under the above rescaling, as does the homogeneous boundary condition on the rigid surface. It is important to notice that the self-similar solution must also satisfy the jump relation (2.6). Since the self-similar rule in the present case is identical to the Fresnel solution discussed by Coulouvrat & Marchiano (2003), the compatibility condition for the shock curve in the self-similar variables can be derived identically.

We depict in figures 3(*a*)–(*c*), the numerical simulation of the KZ equation for the reflected step shock at $X = 1$, 2 and 3 respectively, rescaled in the self-similar variables. A comparison shows that the curves superimpose almost perfectly, which proves that the numerical simulation indeed perfectly captures the self-similar behaviour of the solution. This is confirmed by figure 3(*d*), where the positions of the incident and Mach shock fronts, and of the points of the maximum pressure for the same three distances X are indistinguishable.

For the N-wave, to make the expression (3.8) invariant under the rescaling (4.1) with the invariance condition (4.2) of the KZ equation, we at least need a condition

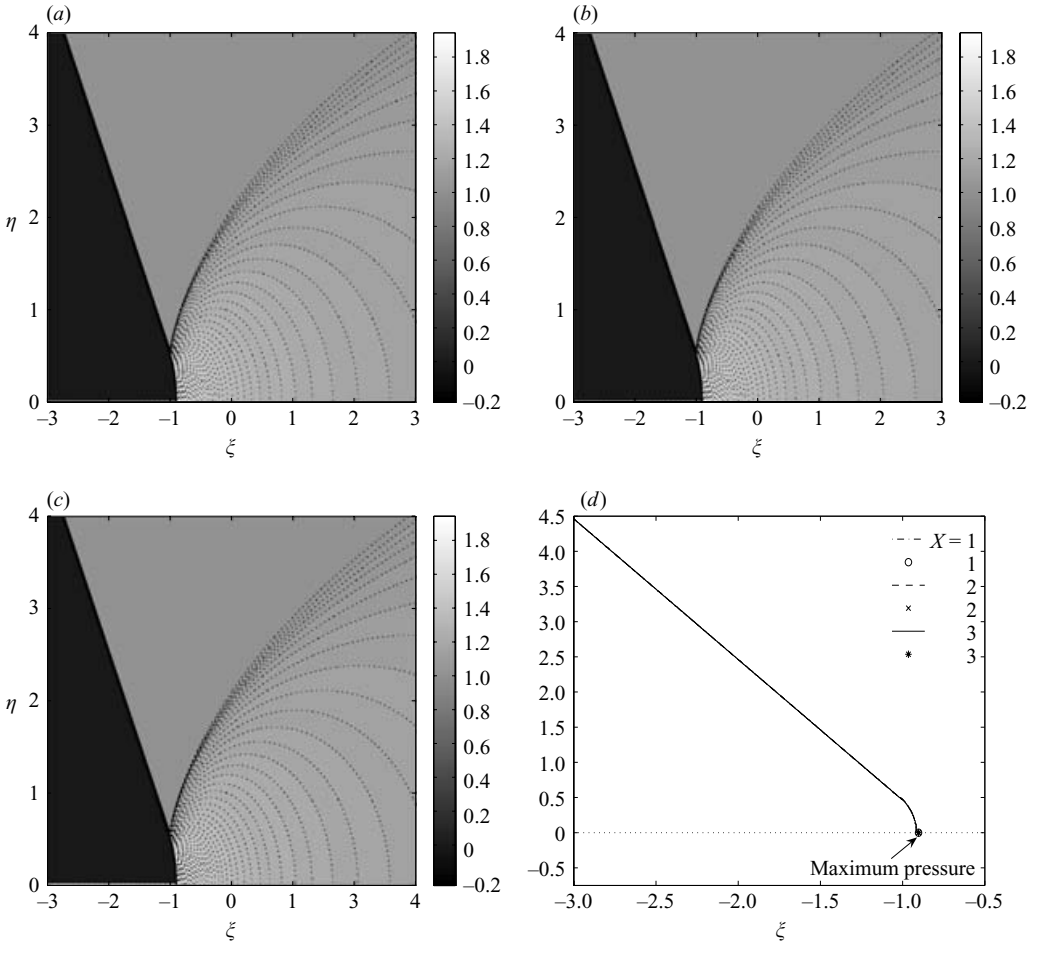

FIGURE 3. Numerical demonstration of the self-similarity property: the pressure field (in grey levels) for $a = 0.5$ and (*a*) $X = 1.0$, (*b*) $X = 2.0$, (*c*) $X = 3.0$. Contour lines are dotted. Plot (*d*) shows that the computed incident and Mach shocks and the position of the maximum pressure for the different values of X are superimposed. All figures are plotted in self-similar coordinates.

which transforms the phase of the wave from

$$\frac{\tau}{\tau^*} + a\frac{Y}{Y^*} + a^2\frac{X}{X^*} - \sqrt{\frac{1}{2} + \frac{X}{2X^*}}$$

to

$$\tau + aY + a^2X - \sqrt{\frac{1+X}{2}}.$$

This is possible only in the case $\tau^* = X^* = Y^* = 1$ and therefore we cannot have a self-similar solution for the N-wave. Similarly we can prove that there is no self-similar solution for the periodic sawtooth wave. However, in the numerical results discussed in § 6, we shall observe that the solutions in these two cases have almost self-similar behaviour for sufficiently small values of X, as the X term in the square roots of the above expressions that prevents self-similarity is negligible.

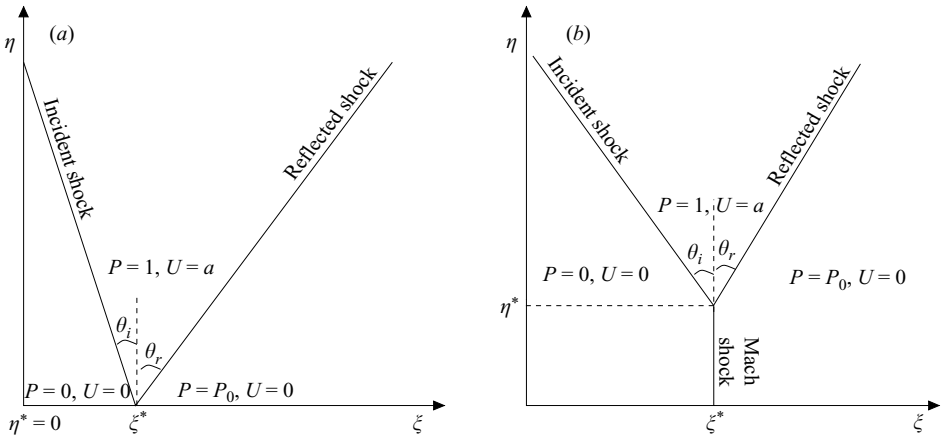

FIGURE 4. (*a*) Regular reflection, (*b*) Mach reflection.

5. Regimes of regular and irregular reflection for step shocks

The purpose of this section is to investigate how the reflection of step shock depends on the value of the critical parameter a introduced in § 3. The reflection is mainly of two types, namely regular reflection and irregular reflection. First we will study theoretically the conditions on a for the transition between these two types of reflection. Then we will review numerically and also classify the different reflection patterns by varying the critical parameter a from infinity to zero.

5.1. *Triple-point condition*

Let us consider the self-similar flow (as proved in § 4) associated with step-shock reflection. We assume that the reflected wave is a shock when it hits the incident shock. In other words, we assume that the triple point does exist and we denote its position in self-similar coordinates as (ξ^*, η^*). We consider the domain $\eta > \eta^*$ above the triple-point and assume classical Mach reflection, in the sense that the incident, reflected and Mach shocks are straight lines separating three constant states. Then the pressure field, the solution of the KZ equation in the domain $(\xi, \eta > \eta^*)$, is given by

$$P(\xi, \eta) = \begin{cases} 0 & \text{if } \xi \leqslant \xi_s^i(\eta), \\ 1 & \text{if } \xi_s^i(\eta) < \xi \leqslant \xi_s^r(\eta), \\ P_0 & \text{if } \xi_s^r(\eta) < \xi, \end{cases} \tag{5.1}$$

where ξ_s^i and ξ_s^r are the incident and reflected shocks respectively and are given by

$$\xi_s^i(\eta) = -a\eta - (a^2 + 1/2) \tag{5.2}$$

for the incident shock according to the boundary condition (3.6) and

$$\xi_s^r(\eta) = b\eta - ((a+b)\eta^* + a^2 + 1/2) \tag{5.3}$$

for the reflected shock.

In (5.3), the parameter b associated with the slope of the reflected shock is defined similarly to the parameter a given in (3.3), but now for the reflected angle θ_r (say) instead of $\theta_i = \theta$ for the incident angle (see figure 4). The change of sign in (5.3) as compared with (5.2) holds for the reflected wave and the constant is chosen so that the two shocks meet at the triple point. In (5.1), P_0 is the dimensionless pressure

behind the reflected shock, which is yet to be calculated. Our problem is to find the condition on b and P_0, as a function of a, such that that the reflected shock satisfies the Rankine–Hugoniot condition. The triple point (ξ^*, η^*) is given by

$$\xi^* = -a\eta^* - \left(a^2 + \tfrac{1}{2}\right). \tag{5.4}$$

The incident shock velocity $\boldsymbol{W}^i$ and the unit normal vector to the incident shock $\boldsymbol{N}^i$ are given by

$$\boldsymbol{W}^i = \left(-\left(a^2 + \tfrac{1}{2}\right), 0\right), \qquad \boldsymbol{N}^i = \frac{1}{\sqrt{1+a^2}}(1, a).$$

The reflected shock velocity $\boldsymbol{W}^r$ and the unit normal vector to the reflected shock $\boldsymbol{N}^r$ are given by

$$\boldsymbol{W}^r = \left(-\left((a+b)\eta^* + a^2 + \tfrac{1}{2}\right), 0\right), \qquad \boldsymbol{N}^r = \frac{1}{\sqrt{1+b^2}}(1, -b).$$

Either of the two Rankine–Hugoniot relations (2.4) and (2.5) for the incident shock gives the value $U_0 = a$. The Rankine–Hugoniot relations for the reflected shock give (2.5) the value $P_0 = 1 + a/b$ and (2.4), finally, the relation between the incident and the reflected angles:

$$(b+a)(2b^2 - 2(\eta^* + a)b + 1) = 0. \tag{5.5}$$

We note here that b is positive, because the reflected shock has to propagate away from the surface. Thus, $b = -a$ is impossible. The other two solutions of (5.5) are

$$b = \frac{(\eta^* + a) \pm \sqrt{(\eta^* + a)^2 - 2}}{2}, \tag{5.6}$$

which results in a real value of b if and only if

$$\eta^* > \sqrt{2} - a, \tag{5.7}$$

in which case both solutions are positive.

As a consequence, triple-point reflection can exist only if the critical parameter a is smaller than $\sqrt{2}$ (so that $\eta^* > 0$). Otherwise, regular reflection must occur and the above calculation of the reflected angle b and of the reflected pressure P_0 is valid with $\eta^* = 0$. For regular reflection and large values of a, the positive branch of (5.6) tends towards $b = a$ and, therefore, $P_0 = 2$ (figure 5). That branch recovers the classical Snell–Descartes law for linear waves (the reflected angle is equal to the incident angle and the pressure doubles at the surface) and is consequently physically admissible. Note however that a significant deviation from the Snell–Descartes law occurs for values of a smaller than about 5. For typical sonic booms or ultrasound in water ($M = 10^{-3}$) this corresponds to angles smaller than 12 degrees. Hence, nonlinear effects will occur even for non-grazing incidence, in the form of a reflected wave that is less grazing than the incident one ($b > a$) and a reflected pressure that is larger than the incident one ($P_0 > 2$). At the critical value, where the largest deviation occurs, $a = \sqrt{2}$, the pressure triples on the surface while the reflected angle is only half the incident one.

5.2. *Regular reflection*

The relation between a and b in the above discussion shows that nonlinearity plays a role in the regular reflection for a moderate value of a (in practice less than 5). This is illustrated in the numerical simulations for $a = 1.5$ and 2.0, which are displayed in

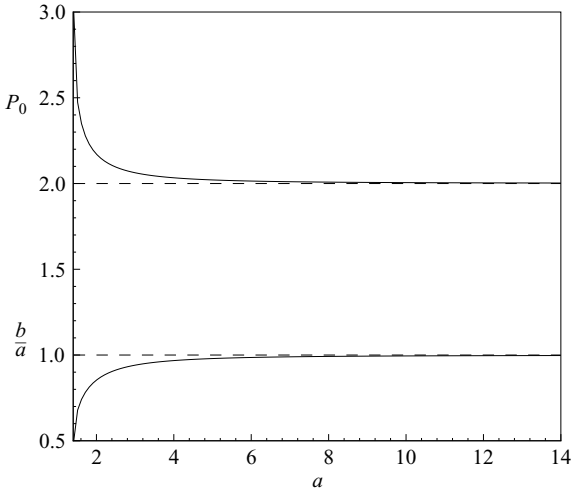

FIGURE 5. Transition from nonlinear to linear (Snell–Descartes) regular reflection. Upper curve, the ratio of total and incident pressures; lower curve, ratio of reflected and incident angles. The linear regular reflection occurs almost for $a > 5$.

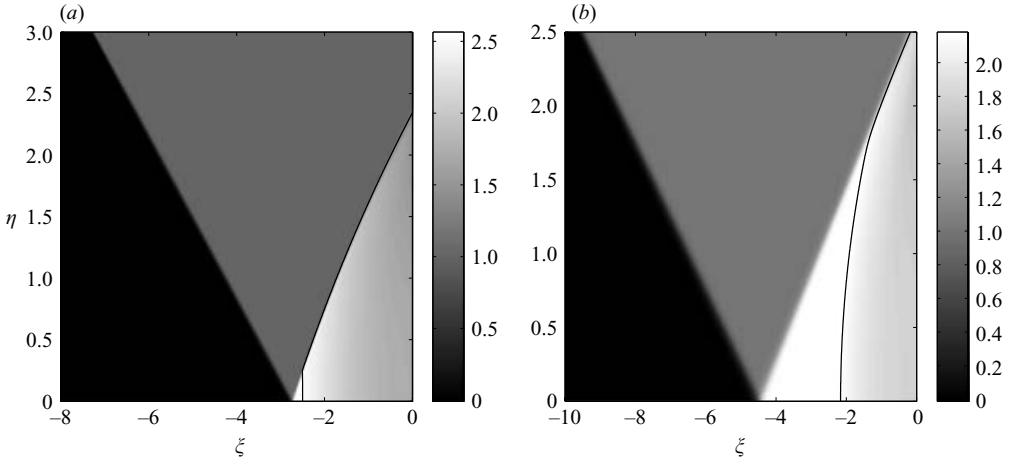

FIGURE 6. Regular reflection: the pressure field (in grey levels) in self-similar variables for (*a*) $a = 1.5$ and (*b*) $a = 2.0$ at $X = 1.0$. The solid curve is the sonic line.

figure 6. Obviously, in the figure the slope of the incident and the reflected shocks in the neighbourhood of the surface are different and the pressure behind the reflected shock is greater than 2. For $a = 1.5$ in figure 6(*a*), the numerical value of the maximum pressure, which is obtained at the reflection point, is 2.5655. From (5.6) we get $b = 1$ and consequently the pressure behind the reflected shock, $P_0 = 1 + a/b$, equals 2.5, which is very close to the numerically obtained maximum pressure. Similarly, for $a = 2$ in figure 6(*b*), the numerical value of the maximum pressure is 2.1821 whereas the theoretical value is 2.1716. Good agreement between theoretical and numerical values will be further illustrated in figure 10.

The theory detailed in § 5.1 is indeed equivalent to the von Neumann (1943) two-shock theory but restricted to the approximate KZ equation. According to the approximations in the theory, shocks are assumed to be perfectly straight and to

separate only states with constant pressure and velocity. However, it is observed in the simulations that these assumptions are valid only in the vicinity of the reflection point. The physical reason for this is the existence of a wave diffracted by the impact of the incident shock at the edge $X = 0$ of the rigid surface. This diffracted wave (neglected in the simplified theory of von Neumann), called the corner signal by Henderson (1987), must have a spherically shaped wavefront (at least in linear acoustics) according to Huyghens' principle; however, because of the parabolic approximation in the KZ equation, the diffracted wavefront here has a parabolic shape. Once the diffracted wave and the reflected shock interact, the reflected shock bends and is now called the diffracted shock. Consequently, the pressure field cannot any more be constant behind it. This behaviour is very visible in figure 6(*b*), where we can clearly see the constant pressure state just behind the reflected shock until the arrival of the diffracted (or corner) wave with its parabolic wavefront. Then the reflected shock begins to bend and the pressure smoothly decays. Because of the self-similarity of the solution, a point with fixed τ and Y but increasingly large X, in physical variables, will correspond in self-similar variables to the vanishing of the ξ and η variables. Therefore, very far from the edge of the reflector the diffracted wave lags very far behind the reflected wave. Ultimately, as $X \to \infty$ the reflected and diffracted fields will be fully separated, and the observer will see only the vicinity of the reflection point where the shocks are straight and the pressure level is constant. This limiting case is simply the one described by the von Neumann two-shock theory, for which the influence of the diffracted wave is discarded. In the linear regime, of course, and in the far-field limit, we would recover Snell–Descartes reflection from an infinite rigid plate.

Finally, it has to be noted that for the Euler equations the slope of the diffracted shock may vanish and then become negative, so that it may propagate backward and hit the rigid surface as seen in figure 1, drawn according to Ben-Dor (1992). However, this inversion of the slope cannot be obtained using the KZ equation, because the paraxial or parabolic approximation prohibits any backward propagation.

The critical value $a_d = \sqrt{2}$ obtained in § 5.1, near which the transition from regular to irregular reflection takes place, is called the deflection point (see Hunter 1991). Another transition condition called the sonic point is obtained using the notion of the sonic line (see below). The system (2.2), (2.3) written in the self-similar variables ξ, η is given by

$$(\xi + P)\frac{\partial P}{\partial \xi} + \eta\frac{\partial P}{\partial \eta} + \frac{\partial U}{\partial \eta} = 0, \tag{5.8}$$

$$-\frac{\partial U}{\partial \xi} + \frac{\partial P}{\partial \eta} = 0. \tag{5.9}$$

The eigenvalues of the above quasi-linear system are $(\eta \pm \sqrt{\eta^2 - 4(\xi + P)})/2(\xi + P)$, which shows that the system (5.8)–(5.9) changes its nature from hyperbolic to elliptic across the parabola

$$\frac{\eta^2}{4} - \xi = P. \tag{5.10}$$

The curve $\eta = 2\sqrt{\xi + P}$ is called the sonic line. The positive side of the parabola is the elliptic region and the negative side is the hyperbolic region. The sonic line is plotted along with each of the numerical solutions for $a = 1.5$ and 2 in figure 6. Note that the sonic line in figure 6(*b*) is extremely close to the diffracted wave, beyond which

the pressure ceases to be constant. Also visible on the figure is the identification of the sonic line with the curved part of the reflected shock. The notion of the sonic line allows us to derive a second transition criterion between regular and irregular reflection. Indeed, the expression (5.10) shows that the reflection point $(\xi^*, 0)$ lies in the hyperbolic region if and only if

$$-P_0 > \xi^*, \tag{5.11}$$

where P_0 is the pressure at the reflected point, which is the maximum pressure in the entire pressure field, as shown in figure 3(*d*).

For regular reflection the reflection point is given by $(-(a^2 + 1/2), 0)$ (see (5.4)). From (5.6) and $P_0 = 1 + a/b$ we have

$$P_0 = a^2 - a\sqrt{a^2 - 2} + 1. \tag{5.12}$$

Thus, the reflection point lies in the hyperbolic region if and only if

$$a^2 - a\sqrt{a^2 - 2} + 1 < (a^2 + 1/2),$$

which implies

$$a > \sqrt{1 + \sqrt{5}/2} = a_s.$$

It is well known that a shock cannot appear in an elliptic region. Thus for regular reflection the reflection point has to lie in the hyperbolic region. The constant a_s is the transition condition in the sense that for $a < a_s$ regular reflection cannot exist. The constant $a_s = 1.4553$ is the sonic point, the value of a at which the reflection point lies right on the sonic line. The values a_s and a_d obtained here are the same as those derived by Brio & Hunter (1992). Note that the detachment constant $a_d = 1.4142$ is very close to the sonic point a_s. Because of this, these two transition conditions are usually considered as equivalent in the literature (see Colella & Henderson 1990), though the reflection pattern between these two extremely close values remains to be explored. Note that a third transition condition called the Crocco point based on the condition that the streamlines behind the reflected shock are approximately straight can also be derived (see Brio & Hunter 1992) and yields the intermediate value $a = 1.4278$.

5.3. *Irregular reflection*

In § 5.1, we proved that for $a < \sqrt{2}$ regular reflection ceases to exist. Indeed from the triple-point condition (5.7) we necessarily have $\eta^* > 0$, which implies that the reflected wave intersects the incident shock above the rigid surface, a pattern known as irregular reflection (here we use the word 'wave' instead of 'shock' as we will see in this section that it is not necessary that the reflected wave is always a shock when it intersects the incident shock). More precisely we will show that there are two different types of irregular reflection observed in our numerical results, which we discuss in this subsections, depending on where, between 0 and $\sqrt{2}$, the value of the critical parameter a lies.

The first regime is observed for values of a between about 0.4 and $\sqrt{2}$. Figure 7(*a*), (*b*) depicts the reflection solution for $a = 1.0$ and 0.7, respectively. In this regime we can clearly see three shocks, namely the incident shock, the reflected shock and the Mach shock. These three shocks meet at the point T, the triple point. While the incident shock is straight, the Mach and the reflected shocks are clearly curved, in contrast with classical Mach reflection. Also, the classical definition of Mach reflection (see Ben-Dor 1992) implies the presence of a slipstream (with discontinuity

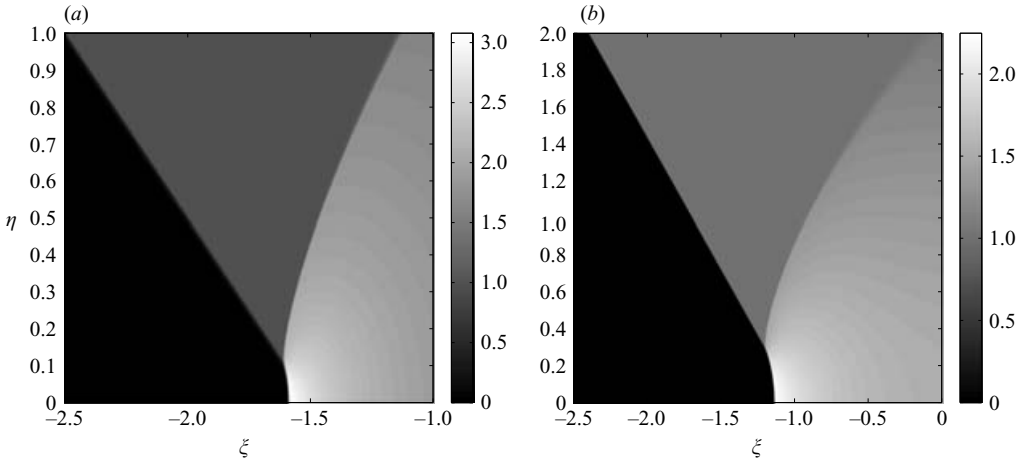

FIGURE 7. Von Neumann reflection: the pressure field (in grey levels) in self-similar variables for (*a*) $a = 1.0$ and (*b*) $a = 0.7$ at $X = 1.0$.

of the entropy, density, temperature and tangential-velocity component) attached to the triple point. Such a slipstream cannot exist in the KZ equation associated with the weak-amplitude approximation, because the temperature and density fluctuations are proportional to the pressure fluctuation, while entropy discontinuity is of third order and therefore can be neglected. Finally, classical Mach reflection occurs for a moderately strong shock (see Henderson 1987 for more discussion on weak and strong shocks). As outlined in the introduction, the question of the existence of a triple shock for weak incident shocks (and therefore for the KZ equation or its equivalent two-dimensional Burgers' equation) remains controversial. We refer the reader to the cited references for the proposed solutions for the classical von Neumann paradox. Again, we recall that the objective of the present work was not to investigate this well-studied phenomenon but to study the transition between the different regimes in the acoustic case and therefore to solve the acoustic von Neumann paradox (see the introduction). So we will label the present regime as von Neumann reflection, according to the terminology most frequently used in the literature, independently of the exact behaviour of the solution near the triple point.

For smaller values of parameter a, the reflected shock progressively weakens up to complete disappearance. This is illustrated by figure 8, which shows the pressure field at $a = 0.1$. Here it is clear that the reflected wave field is simply a smooth compression wave ahead of the incident shock. The smaller the value of the parameter a, the weaker this wave will be, up to complete disappearance for $a = 0$. This reflection regime with no reflected shock at all has never been observed, to our knowledge. It is completely opposite to the Snell–Descartes linear regime, in which the whole pressure field is completely in the hyperbolic domain, with a perfectly straight reflected shock and a sonic line pushed away at infinity. On the contrary, in the present regime there is no reflected shock and almost all the reflected pressure field lies in the elliptic domain, as can be seen in figure 8 where the sonic line has been drawn. Note however that an extremely small part of the reflected wave lies in the hyperbolic region. The question therefore arises whether there exists a reflected shock of very small amplitude, as hypothesized by Hunter & Brio (2000). Our numerical simulations show that, whatever the grid refinement of the numerical domain (up to five times more than that used for figure 8), there is absolutely no change in the numerical

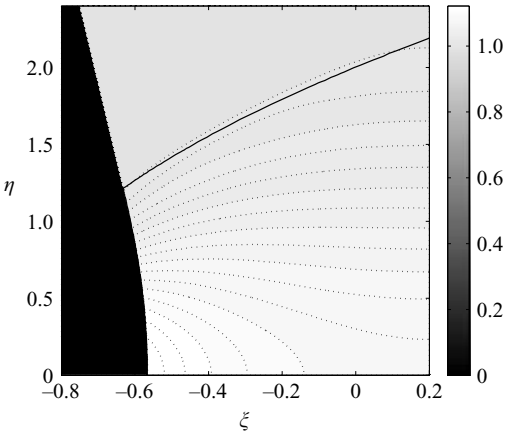

FIGURE 8. Weak von Neumann reflection: the pressure field (in grey levels) in the self-similar variables for $a = 0.1$ and $X = 1$. Contour lines are dotted and the sonic line is solid.

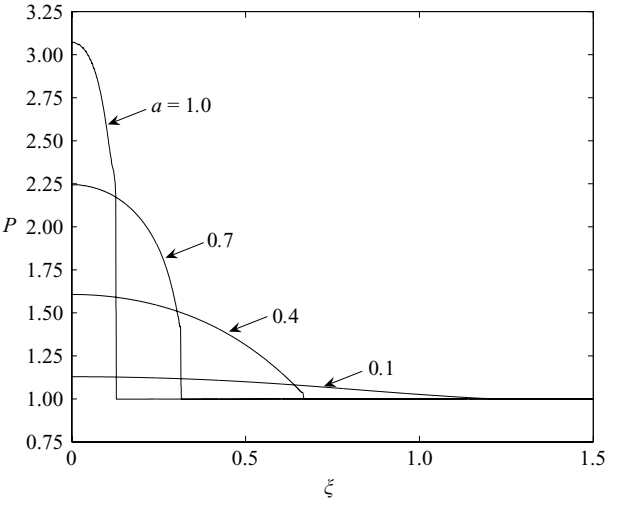

FIGURE 9. The pressure amplitude just behind (by five grid points) the incident and Mach shocks, at $X = 1$ and $a = 0.1$–1.0 with step 0.3. Both the maximum pressure amplitude (obtained at the rigid surface) and the shock strength increase with increasing a. The strength of the shock is very small for $a = 0.4$, around which the transition from von Neumann to weak von Neumann reflection is expected to take place. The profile for $a = 0.1$ is smooth.

solution, which remains continuous. So we believe that, for small values of the parameter a, no reflected shock does exist.

We label this new regime weak von Neumann reflection, in reference to a paragraph in von Neumann (1943) where he raises the problem of the acoustic limit. The transition between von Neumann and weak von Neumann reflection is illustrated by figure 9, which shows the pressure variation along (actually just behind) the incident and Mach shocks for $a = 0.1$ to 1.0. We clearly observe the existence of a pressure jump (down to the constant value 1) associated with the triple point for values of a greater than or equal to 0.4. In contrast, for smaller values of a the curves are

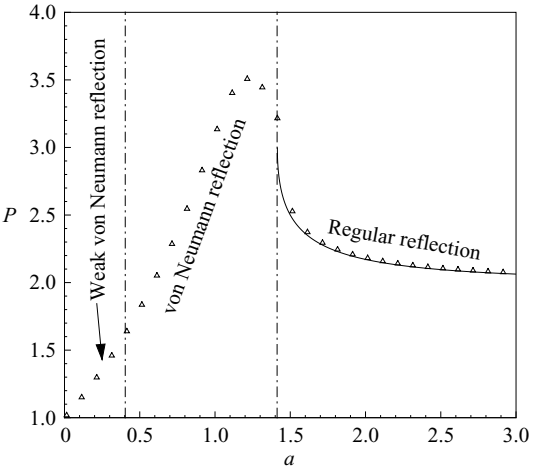

FIGURE 10. Solution of the von Neumann acoustic paradox illustrated by maximum overpressure plotted as a function of the critical parameter a: the transition from Snell–Descartes to perfectly grazing incidence involves, successively, regular, von Neumann and weak von Neumann reflections. The solid line corresponds to the weak two-shock theory and the symbols to the numerical computations.

continuous (for clarity, only the value $a = 0.1$ is displayed but this has been checked also for $a = 0.2$ and 0.3), thus indicating that there is no reflected shock in direct contact with the incident one. From the numerical results, it can also be observed that the arclength of the Mach shock decreases as the value of a increases, which eventually results in a regular reflection for a sufficiently large value of a ($\geqslant\sqrt{2}$), as already discussed in §§ 5.1 and 5.2.

As mentioned in the introduction, von Neumann remarked that the transition from the well-known Snell–Descartes-law region to that of a vanishing reflected wave (for $a = 0$) is singular, in the sense that the former is valid at any grazing angle except the zero angle, where there cannot be any reflected wave. This singular transition was stated as an acoustic paradox by von Neumann. In his original paper, von Neumann expected a behaviour for extremely weak acoustic shock waves different from that for stronger shocks. In the acoustic case, he expected a monotonic decrease of the reflected amplitude with grazing angle, while he described a more complex pattern in the other case. Our present study proves that on the contrary there is no fundamental difference between an acoustic shock wave and other stronger shocks. This is illustrated by figure 10, which summarizes the different regimes of reflection observed above by plotting the (dimensionless) maximum total pressure as a function of the parameter a (or equivalently as a function of the grazing angle for an incident shock wave of fixed amplitude). Obviously, though we are dealing here only with weak acoustic shocks, the transition from the linear Snell–Descartes laws (maximum total pressure equal to 2 for high values of the parameter a) to the perfectly grazing case (maximum total pressure equal to 1) is not monotonic. When decreasing the value of the parameter a, we observe an increase in the pressure, first according to the regular reflection law (a continuous line corresponding to (5.12)). Below the critical value $a = \sqrt{2}$ the increase keeps on, now in the von Neumann reflection regime. The maximum, about 3.5 times the incident amplitude, is reached slightly below the critical value, at about $a = 1.2$. It is only below this value that monotonic behaviour is finally observed. Keeping on decreasing the parameter a, the maximum pressure falls down progressively, finally

entering the weak von Neumann regime at around $a = 0.4$. Note also that the number of shocks involved in the reflection varies from two (regular reflection) to three (weak Mach reflection) and finally to one (weak von Neumann reflection). Of course, for a very small shock amplitude this complex transition will occur only over an extremely small range of grazing angles (in practice a few degrees). It may be difficult to observe, and all the more so since other competing effects than nonlinearities may affect the process, such as viscosity, thermal effects, surface roughness, curvature or elasticity. However, this nonlinear non-monotonic behaviour has been observed experimentally for ultrasonic shock waves produced in water (see Baskar, Coulouvrat & Marchiano 2006). So, we can conclude here that the two extreme linear regimes (perfectly grazing and Snell–Descartes) can indeed be matched continuously, as expected by von Neumann, but unexpectedly this matching is inherently nonlinear and non-monotonic.

6. Unsteady reflection of N-waves and sawtooth waves

The discussion in § 5 showed that the reflection of a weak-amplitude step shock can lead to different regimes of reflection. However, step shocks are not very realistic for acoustic waves and the question remains open about the reflection regimes of more complex but physically relevant wave profiles. The objective of the present section is to investigate whether irregular reflections also occur for realistic acoustic waves. We have selected the cases of N-waves (§ 6.1) and periodic sawtooth waves (§ 6.2).

6.1. *N-waves*

We consider the incident shock to be an N-wave, as defined in (3.8). Unlike the step shock discussed in § 5 we have here two shocks, the leading shock with a compression from the ambient state and the rear shock with a recompression back to the ambient state, the two being connected by an expansion wave. When the leading shock encounters the wedge surface, reflection takes place. As a consequence the associated reflected wave interacts nonlinearly with the expansion wave and thus affects the reflection of the rear shock. This interaction is an additional phenomenon compared with the simplified step-shock case.

Figure 11(*a*)–(*d*) depicts the reflection solution for $a = 0.5$ (a value chosen as representative of irregular reflection in the step-shock case) and for values of the distance $X = 0.603$, 1.8593, 5 and 15 from the edge of the plate respectively, covering a sufficiently long propagation distance. In figure 11(*a*), we can clearly observe the irregular (von Neumann-type) reflection of both the leading and the rear shocks. At such small values of X, the main difference from the step-shock case is that the incident rear shock is slightly curved because of the interaction with the reflected wave. If we decrease the value of the parameter a then we observe also, as for the step shock, weak von Neumann reflection around $a = 0.4$ (not shown here) for sufficiently small values of X. This indicates (as remarked at the end of § 4) that, near the tip of the plate, the reflection of the N-wave is similar to the step-shock case. However, because the N-wave case is not self-similar (as proved in § 4), this cannot be true all along the propagated wave.

From (3.8), we see that the incident shock amplitude decreases with distance as $O(1/\sqrt{X})$. This decrease results in an increase of the local 'true' value of the parameter a and therefore tends to decrease the length of the Mach stem. This effect competes with the tendency of the Mach stem to increase in length, as for a step shock, because of self-similarity. Therefore, for an N-wave we initially observe a behaviour similar to step shocks with an increase of the length of the Mach stem. This is named direct

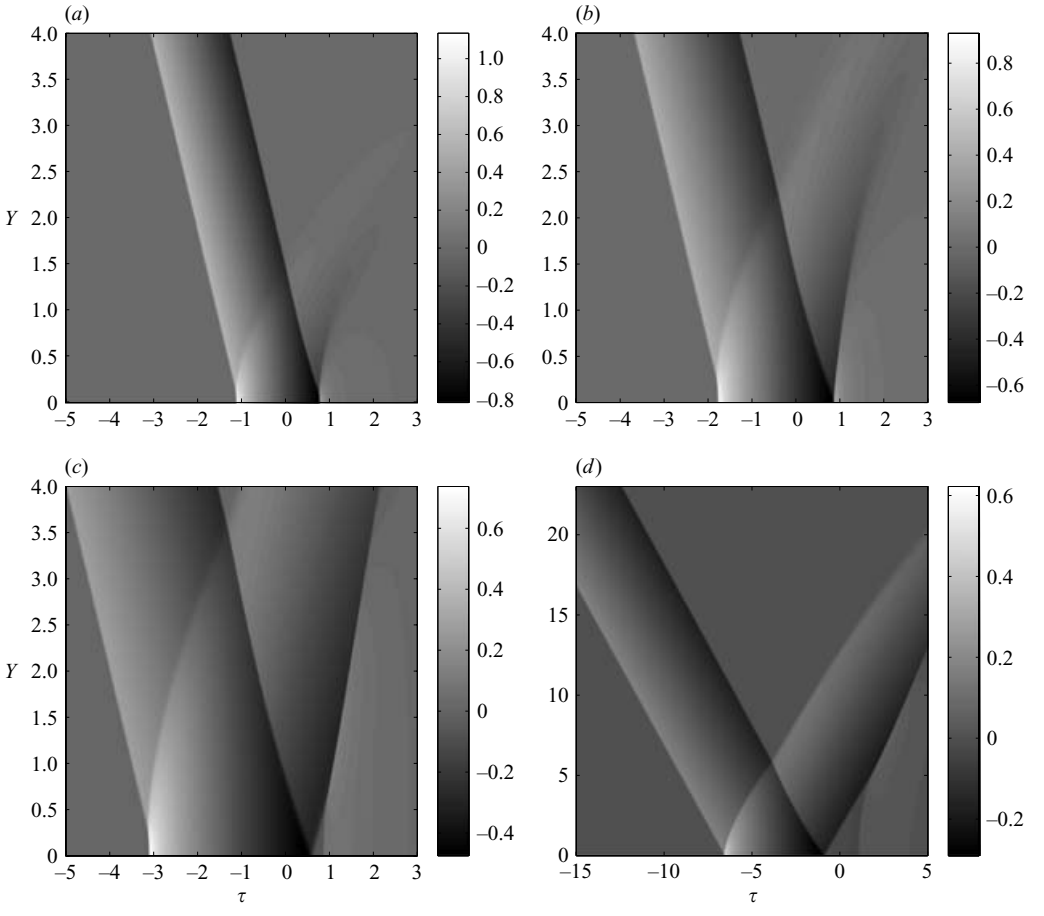

FIGURE 11. Unsteady irregular reflection of an N-wave: the pressure field (in grey levels) as a function of the (τ, Y)-variables for $a = 0.5$ at (*a*) $X = 0.603$, (*b*) 1.8593, (*c*) 5.0 and (*d*) 15.0.

irregular reflection. As the pressure amplitude decreases, as can be seen by comparing the length of the Mach stem in figures 11(*a*)–(*c*), the latter then reaches a maximum before progressively decreasing, a regime named inverse irregular reflection. Finally, when the triple point touches the rigid surface at a finite X value called the termination point, irregular reflection is replaced by regular reflection. This final reflection regime for the head shock is observed in figure 11(*d*). A similar behaviour will be detailed, in § 6.3, for a periodic sawtooth wave. From the above discussion we see that there are two types of irregular reflection configuration that take place for the leading shock. Courant & Friedrichs (1948) categorized these two reflections for the step shock, and the names 'direct' or 'inverse irregular reflection' and 'termination point' were suggested by them.

It has also been observed from our numerical experiments that the value of the termination point and the maximum of the triple-point trajectory both decrease as the value of a increases, as logically expected since we are closer to regular reflection. Thus for a sufficiently large value of a, which is observed approximately as 0.8, there is no irregular reflection at all, the head shock reflecting regularly all along the plate. Thus, with this study, we categorize the types of reflection for the leading

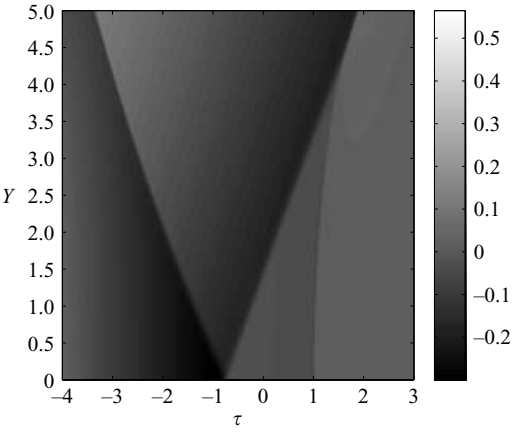

FIGURE 12. Transitioned regular reflection of type 2: a closer view of the pressure field (in grey levels) of the rear shock for $a = 0.5$ at $X = 15.0$.

shock as regular reflection (for a greater than approximately 0.8), dynamical irregular reflection (for a lying between approximately 0.4 and 0.8) and weak reflection (for a less than approximately 0.4), where initially the reflected wave is not a shock. The exact transition condition between these three types of reflection and the presence of any further types of irregular reflection are yet to be investigated. Note however that this categorization is different from the step-shock case, where it remains valid all along the plate because of self-similarity. Here, because of the incident wave amplitude decay, the reflection process is now dynamical. Whatever the regime it begins with, it always converges towards regular reflection and ultimately towards the linear Snell–Descartes case.

The reflection phenomena for the rear shock of the N-wave is somewhat different from the leading shock discussed above. Initially we observe the same succession of direct and inverse irregular reflections, the only difference being that the length of the Mach stem remains smaller than for the head shock (though the shocks themselves are of the same amplitude). Inverse irregular reflection terminates when the triple point hits the rigid surface. The difference between the leading and the rear shocks occurs after the termination. Indeed for the rear shock, we observe an additional shock, which is called the secondary reflected shock, that detaches from the reflected shock right at the termination point. Our interpretation is that this new shock emerges from the impact on the rigid surface of the reflected shock when the latter collides with the surface at the termination point. This new kind of reflection therefore has to create a new reflected shock, which appears as a secondary reflected shock. For this secondary reflection pattern, the primary reflected shock plays the role of the incident shock, the secondary reflected shock plays the role of the reflected shock and the two merge into a single reflected shock, which plays the role of the Mach shock, at a new, secondary, triple point. The only difference from classical weak Mach reflection is that now the Mach shock extends away from the surface. This reflection pattern is visible in figures 11(c), (d). A closer view is provided by figure 12, where all four shocks are visible (the incident rear shock, the primary reflected shock, the secondary reflected shock and the merging of the last two into a Mach shock). Figure 13 displays the pressure–time profile for $a = 0.5$ and $X = 15$ at the rigid surface, where we can clearly observe this new secondary reflected shock at the trailing part of the wave profile.

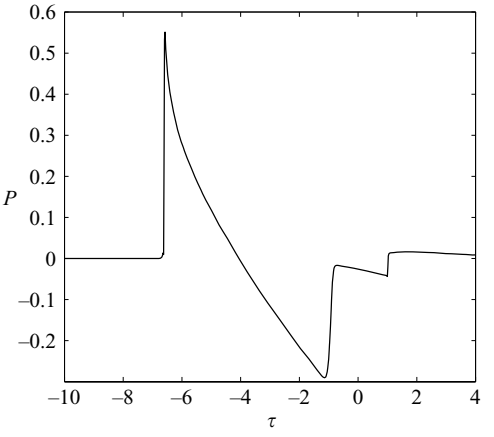

FIGURE 13. Pressure vs. time waveform on the rigid surface for $a = 0.5$ at $X = 15.0$, which clearly shows the presence of the secondary reflected shock.

This secondary reflection appears absolutely similar to the von Neumann reflection described in § 5. Indeed, we can observe from figures 11(*d*) and 12 that here the primary reflected shock (playing the role of an incident shock) seems almost straight, the Mach shock is slightly curved and the secondary reflected shock has to be strongly curved, to match the inclination of the secondary Mach shock at one end and the normal boundary condition at the surface at the other end. Finally, for long distances the terminated reflection of the incident rear shock remains regular (we expect it to fit the linear Snell–Descartes law at very large distances, where the amplitude will be small). Because of the nature of the terminated reflection, this type of reflection is called transitioned regular reflection of type 2.

Transitioned regular reflection of type 2 was described by Takayama & Ben-Dor (1985) for step-shock reflection at a concave rigid surface. Here the curvature of the surface has been replaced by a decrease in the amplitude of the incident wave, but both are similar in the sense that the local critical parameter a is not constant but increases along the reflecting surface. Also, the two cases are similar because in each case (step-shock reflection on a concave surface or the reflection of a decreasing-amplitude wave along a plane surface) the ambient state behind the incident shock is constant. This is not so for the leading shock of the N-wave, for which this type of transitioned regular reflection is not observed, with no secondary reflected shock. The transitioned regular reflection observed for the leading shock of the N-wave is therefore called type 1, to distinguish it from type-2 reflection, that observed for the rear shock. We will see in the following subsections that type-1 reflection is also observed for a periodic sawtooth wave.

6.2. *Periodic sawtooth wave*

Finally, we consider an incident shock that is a periodic sawtooth wave as given in (3.10), with the objective of investigating the interactions between the successive incident and reflected shocks. Figure 14 shows the propagation of a periodic sawtooth wave for $a = 0.5$ at various distances. As for the N-wave, we observe the existence of an unsteady irregular reflection due to the competition between nonlinear effects at grazing angle and the decrease in the amplitude. This results in a direct and then inverse irregular reflection, up to termination, and then a return to the regular reflection. The trajectory of the triple point is illustrated in figure 15 for $a = 0.5$

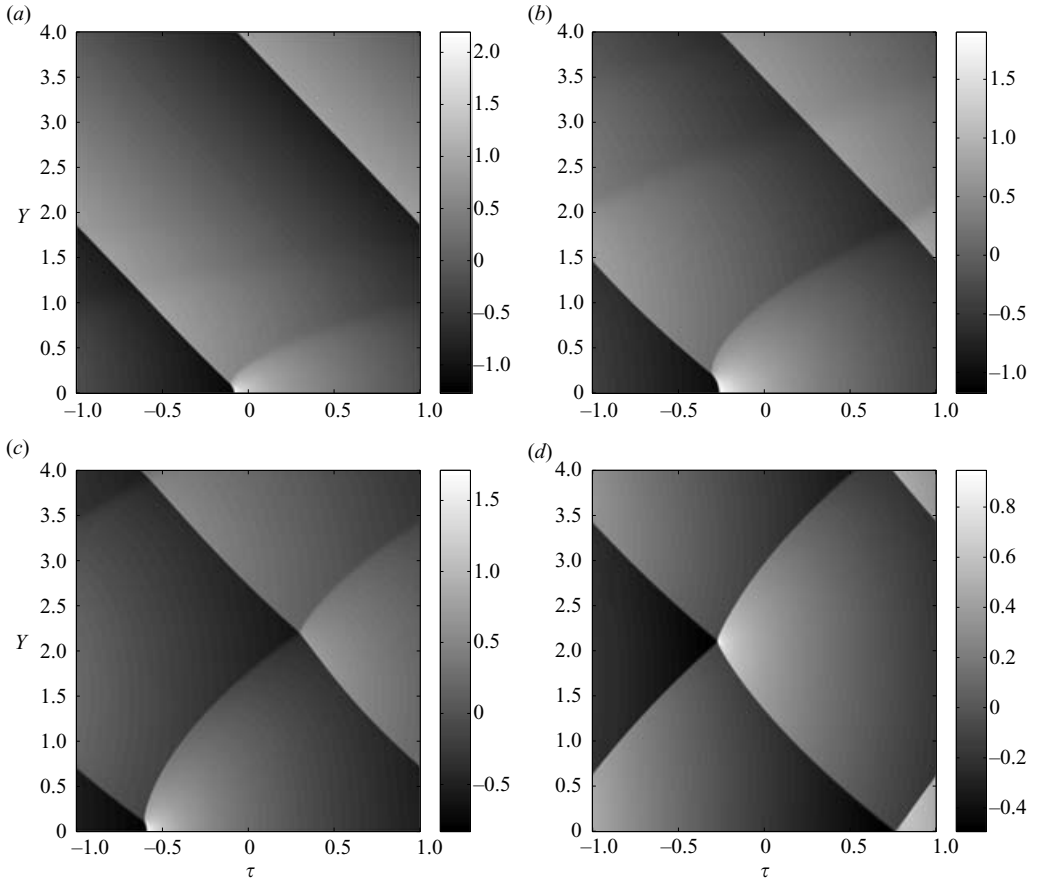

FIGURE 14. Unsteady irregular reflection of a periodic sawtooth wave: the pressure field (in grey levels) in (τ, Y)-coordinates for $a = 0.5$ at (a) $X = 0.2462$, (b) $X = 1.0$, (c) $X = 2.5075$ and (d) $X = 5.0201$.

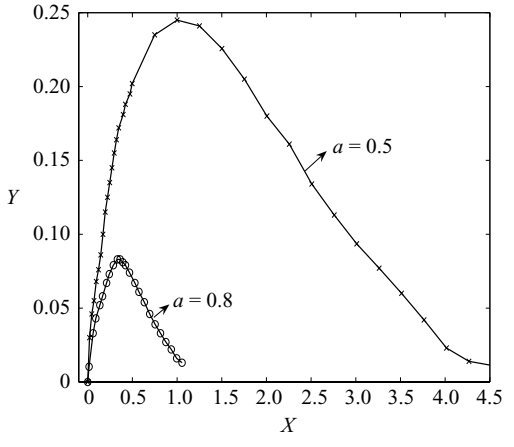

FIGURE 15. Numerically traced triple point trajectory of the sawtooth wave for $a = 0.5$ (with solid line and symbol $\times$) and $a = 0.8$ (with solid line and symbol $\circ$).

and $a = 0.8$. The maximum of the length of the Mach stem is obtained at almost $X = 1$ for $a = 0.5$ and almost $X = 0.3$ for $a = 0.8$, with a rather rapid (almost linear as for the self-similar step-shock case) increase during the direct phase for small X and then a slower decrease, up to X about 4.5 for $a = 0.5$ and up to X about 1 for $a = 0.8$ (the termination point is not so clearly traced from our numerical result because of numerical diffusion near the surface). It is noticeable that the position of the termination point is highly variable with the pressure waveform, with a value of about 15 for the leading shock of the N-wave and only 1.8 for the rear shock of the N-wave (for $a = 0.5$). However, qualitatively, the nature of the triple-point trajectories are similar to that studied by Ben-Dor & Takayama (1985) experimentally for a step shock grazing over a cylindrical concave surface. Beyond the termination point, the reflection phenomenon is a transitioned regular reflection of type 1, with no secondary reflection (the solution was computed up to $X = 8$ without any secondary shock being observed). In this sense, it is very similar to the leading shock of the N-wave. Once again, we think that this is due to the fact that the incident pressure field behind the shock is not constant (here because of the periodic nature of the wave), which seems to prevent any secondary reflection. Finally, it is to be noticed in figure 11(*d*) that beyond the termination point the maximum amplitude of the pressure field no longer lies at the surface but is now at the intersection between the reflected shock and the next incident shock. Clearly visible also is the curvature of the incident shocks due to the interaction with the reflected wave.

For transient nonlinear acoustic waves of finite energy, because shock waves are dissipative processes, the energy decreases. As a consequence, in contrast with step shocks, the reflection phenomenon cannot be self-similar; it is necessarily unsteady along the reflector and it will unavoidably converge towards regular reflection and finally to linear Snell–Descartes reflection. This was observed above for the transition process from Mach to regular reflection, both for the N-wave and the sawtooth wave. It is also true if we initiate the process with weak von Neumann reflection, as illustrated in figure 16 for a sawtooth wave with $a = 0.3$. The computations at different distances clearly show the transition from the weak von Neumann reflection for small X values (figure 16*a*, with $X = 2.0040$) to von Neumann reflection for intermediate X values (figure 16*c*, with $X = 6.0$), the transition occurring around $X = 3.6$ (figure 16*b*). Finally, for very large distances the reflection ultimately evolves into regular reflection (figure 16*d*, with $X = 16.03$). Note here again that the maximum amplitude is no longer observed to be on the surface.

So, for realistic waveforms, even for fixed incidence angle, no single reflection regime can be observed; the loss of energy of the incident wave will necessarily imply the transition from weak von Neumann to Mach to regular and finally to Snell–Descartes reflection. This transient behaviour may explain why these nonlinear reflection regimes have not been observed for acoustic shock waves until very recently (see Baskar, Coulouvrat & Marchiano 2006).

7. Conclusion

Obliquely grazing shock-wave reflection over a rigid surface has been studied from the acoustic point of view. Three types of incident wave have been considered, namely the step shock, the N-wave and the periodic sawtooth wave. The shock amplitude and the grazing angle were assumed to be very weak and in a ratio (measured by the critical parameter a) ensuring the proper balance between nonlinear and diffraction effects. This critical parameter is the key parameter of the problem in the sense

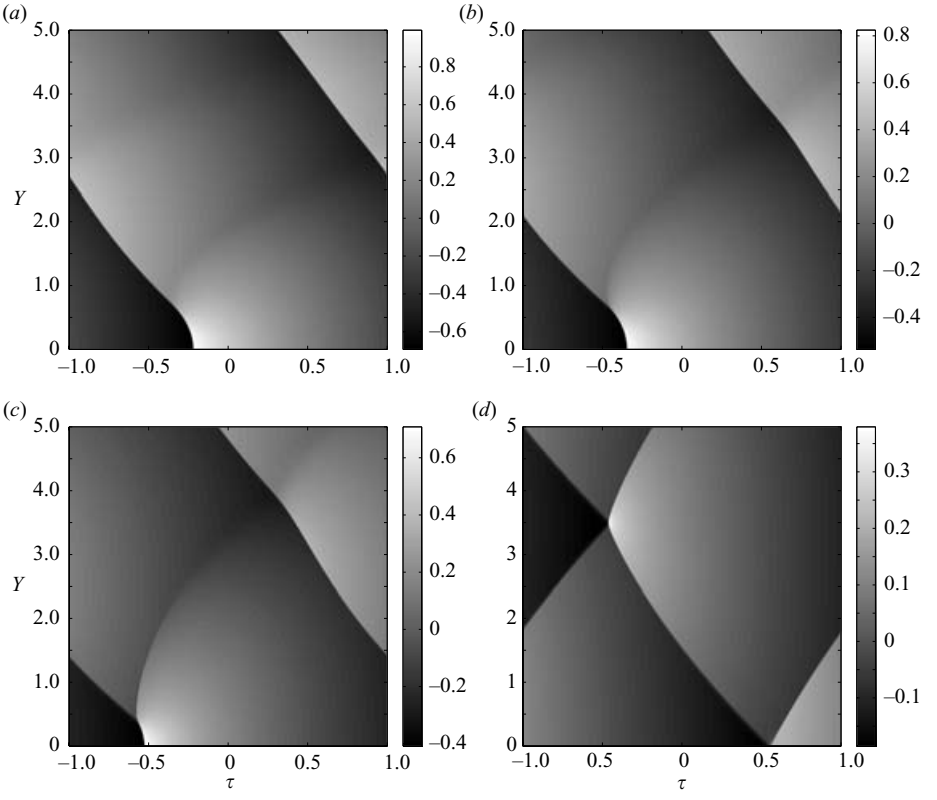

FIGURE 16. Unsteady irregular reflection of a periodic sawtooth wave: the pressure field (in grey levels) in (τ, Y)-coordinates for $a = 0.3$ at (a) $X = 2.0040$, (b) $X = 3.6072$, (c) $X = 6.0120$ and (d) $X = 16.0321$.

that it categorizes the nature of the reflection. Though non-realistic from an acoustic viewpoint because it is of infinite energy, the step-shock case was studied first, precisely for the purpose of categorization of the reflection regimes, on the basis of the self-similar property of the problem. Four different types of reflection, ranging from very strong to very weak reflection, have been observed and their transition studied both theoretically and numerically. Classical linear Snell–Descartes reflection takes place only for relatively large values of the critical parameter, $a > 5$. The Snell–Descartes laws have been generalized (according to weak-shock theory) to nonlinear regular reflection for values of a smaller than 5 but larger than $\sqrt{2}$. The regular reflection is characterized by a reflection angle and a reflected pressure amplitude larger than the incident ones. A transition condition from regular to irregular reflection is obtained theoretically at $a = \sqrt{2}$, which is the classical detachment point obtained by Brio & Hunter (1992) (another transition condition almost equivalent and called the sonic condition can also be recovered). We categorize irregular reflection into two types. The first is von Neumann reflection, observed for $0.4 \leqslant a < \sqrt{2}$, with the existence of a triple point. As we decrease the value of a further, we observe the complete disappearance of the reflected shock, the reflected wave now being only a small-amplitude smooth-compression wave. We have suggested that this new type of reflection should be named weak von Neumann reflection. The continuous transition between these four regimes provides a nonlinear solution to the acoustic von Neumann paradox, according to

which the Snell–Descartes laws are singular. However, in contrast with the von Neumann conjecture, this transition is not monotonic. For instance, the maximum total pressure is about 3.5 around $a = 1.2$ for the intermediate von Neumann regime, much larger than the two extreme values, 2 (for Snell–Descartes at $a = \infty$) and 1 (for a perfectly grazing shock at $a = 0$).

For the acoustically more realistic cases of an N-wave or a periodic sawtooth wave, the step-shock categorization remains valid. However, a key difference is that the process is now unsteady because of the energy loss of the incident shock. Indeed, for a given initial value of the critical parameter, the reflection patterns all along the plate will evolve from the initial pattern (whatever it is) to the regular reflection regime and ultimately to the linear Snell–Descartes limit. For instance, beginning with the weak von Neumann regime at the tip of the plate, we will successively observe transitions to von Neumann reflection and then to regular reflection. We therefore recover types of transition similar to those categorized in the literature in the case of a step shock reflecting over a concave surface. Here the role of the surface curvature is simply replaced by the amplitude decay of the incident wave. In particular, we recover what we call type-2 transitioned regular reflection, in which a secondary reflection takes place. However, this is observed only for the rear shock of the N-wave while for all other cases (the leading shock of the N-wave or the periodic sawtooth wave), this transition is only of type 1, with no secondary reflection. This kind of transition (type 1) has never been described before, according to our knowledge. We assume that this is due to the fact that the incident flow behind the incident shock is not constant, which seems to prevent the type-2 transition. As a consequence, this latter transition seems to be rather exceptional.

The present study has been restricted to a rather idealized situation despite the fact that the incident signals are more complex than a step shock. Indeed, for acoustic applications it would be necessary to take into account several effects that have been neglected here. Surface curvature would compete with amplitude decay. For a concave surface, as for the step-shock situation described in the literature, we expect the curvature to accelerate the transition to regular reflection. In contrast, a convex surface would slow down this transition and we may imagine a special surface design that would exactly compensate nonlinear attenuation. Surface roughness is also expected to affect the process significantly, owing to hysteresis effects, as has already been studied for step shocks (see Ben-Dor 1992). Finally, probably the most significant effect will come from the surface elasticity. Indeed, it is well known that, for a grazing incident wave in a fluid over an elastic medium with transverse wave speed larger than the speed of sound (the common case for metallic materials), total reflection takes place with a reflection coefficient approaching -1 instead of the value $+1$ that applies for a rigid reflector. So we therefore expect this case to be closer to that of reflection at a pressure-release interface. However, the pressure-release reflection of shock waves produces inverted shocks that violate the second law of thermodynamics and that immediately break into expansion fans. Therefore, however rigid the reflector, we expect dramatic differences from the present ideal rigid case.

The first author benefited from a postdoctoral fellowship from the Ministère Délégué à la Recherche, France (décision 140, 2004). The authors are grateful to Dr Jean-Louis Thomas (Centre National de la Recherche Scientifique UMR 7855, Institut des Nano-Sciences de Paris, Université Pierre et Marie Curie – Paris 6) for his valuable suggestions. The anonymous reviewers should be thanked for their helpful comments and suggestions about the bibliography of the present work.

REFERENCES

Auger, T. & Coulouvrat, F. 2002 Numerical simulation of sonic boom focusing. *AIAA J.* **40**, 1726–1734.

Baskar, S., Coulouvrat, F. & Marchiano, R. 2006 Irregular reflection of acoustic shock waves and von Neumann paradox. In *Innovations in Nonlinear Acoustics (Proceedings of 17th International Symposium on Nonlinear Acoustics)* (ed. A. A. Atchley, V. W. Sparrow & R. M. Keolian), pp. 536–539. AIP.

Ben-Dor, G. 1987 A reconsideration of the three-shock theory for a pseudo-steady Mach reflection. *J. Fluid Mech.* **181**, 467–484.

Ben-Dor, G. 1992 *Shock Wave Reflection Phenomena*. Springer.

Ben-Dor, G. & Takayama, K. 1985 Analytical prediction of the transition from Mach to regular reflection over cylindrical concave wedges. *J. Fluid Mech.* **158**, 365–380.

Ben-Dor, G. & Takayama, K. 1992 The phenomena of shock wave reflection – a review of unsolved problems and future research needs. *Shock Waves* **2**, 211–223.

Birkhoff, G. 1950 *Hydrodynamics, A Study in Logic, Fact and Similitude*. Princeton University Press.

Brio, M. & Hunter, J. K. 1992 Mach reflection for the two-dimensional Burgers' equation. *Physica* D **60**, 194–207.

Colella, P. & Henderson, L. F. 1990 The von Neumann paradox for the diffraction of a weak shock waves. *J. Fluid Mech.* **213**, 71–94.

Coulouvrat, F. & Marchiano, R. 2003 Nonlinear Fresnel diffraction of weak shock waves. *J. Acoust. Soc. Am.* **114**, 1749–1757.

Courant, R. & Friedrichs, K. O. 1948 *Supersonic Flows and Shock Waves*. Interscience.

Guderley, K. G. 1962 *The Theory of Transonic Flow*. Pergamon.

Hamilton, M. F. & Blackstock, D. T. 1998 *Nonlinear Acoustics*. Academic Press.

Henderson, L. F. 1987 Region and boundaries for diffracting shock wave systems. *Z. Angew. Math. Mech.* **67**, 73–86.

Henderson, L. F., Crutchfield, W. Y. & Virgona, R. J. 1997 The effects of thermal conductivity and viscosity of argon on shock waves diffraction over rigid ramps. *J. Fluid Mech.* **331**, 1–36.

Hunter, J. K. 1991 Nonlinear geometrical optics. In *Multidimensional hyperbolic problems and computations* (ed. A. J. Majda & J. Glimm), pp. 179–197. IMA Volumes in Mathematics and its Applications Vol. 29, Springer.

Hunter, J. K. & Brio, M. 2000 Weak shock reflection. *J. Fluid Mech.* **410**, 235–261.

Kobayashi, S., Adachi, T. & Suzuki, T. 1995 Examination of the von Neumann paradox for a weak shock wave. *Fluid Dyn. Res.* **17**, 13–25.

Kobayashi, S., Adachi, T. & Suzuki, T. 2004 Non-self-similar characteristics of weak Mach reflection: the von Neumann paradox. *Fluid Dyn. Res.* **35**, 275–286.

Lee, Y. S. & Hamilton, M. F. 1995 Time-domain modeling of pulsed finite-amplitude sound beams. *J. Acoust. Soc. Am.* **97**, 906–917.

Mach, E. 1878 Über den Verlauf von Funkenwellen in der Ebene und im Raume. *Sitzungsbr. Akad. Wiss. Wien* **78**, 819–838.

Marchiano, R., Coulouvrat, F. & Grenon, R. 2003 Numerical simulation of shock wave focusing at fold caustics, with application to sonic boom. *J. Acoust. Soc. Am.* **114**, 1758–1771.

Marchiano, R., Coulouvrat, F. & Thomas, J. L. 2005 Nonlinear focusing of acoustic shock waves at a caustic cusp. *J. Acoust. Soc. Am.* **117**, 566–577.

McDonald, B. E. & Kuperman, W. A. 1987 Time domain formulation for pulse propagation including nonlinear behavior at a caustic. *J. Acoust. Soc. Am.* **81**, 1406–1417.

von Neumann, J. 1943 Oblique reflection of shocks. In *John von Neumann Collected Work, vol. 6 (1963)* (ed. A. H. Taub), pp. 238–299. Pergamon.

Skews, B. W. 1972 The flow in the vicinity of the three shock interaction. *CASI Trans.* **4**, 99–107.

Skews, B. W. & Ashworth, J. T. 2005 The physical nature of weak shock wave reflection. *J. Fluid Mech.* **542**, 105–114.

Sternberg, J. 1959 Triple-shock-wave intersections. *Phys. Fluids* **2**, 179–206.

Tabak, E. G. & Rosales, R. R. 1994 Focusing of weak shock waves and the von Neumann paradox of oblique shock reflection. *Phys. Fluids* **6**, 1874–1892.

Takayama, K. & Ben-Dor, G. 1985 The inverse Mach reflection. *AIAA J.* **23**, 1853–1859.

Tesdall, A. M. & Hunter, J. K. 2002 Self-similar solutions for weak shock reflection. *SIAM. J. Appl. Maths* **63**, 42–61.

Vasil'ev, E. & Kraiko, A. 1999 Numerical simulation of weak shock diffraction over a wedge under the von Neumann paradox conditions. *Comput. Maths. Math. Phys.* **39**, 1335–1345.

Zabolotskaya, E. A. & Khokhlov, R. V. 1969 Quasi-plane waves in the nonlinear acoustics of confined beams. *Sov. Phys. Acoust.* **15**, 35–40.

Zakharian, A. R., Brio, M., Hunter, J. K. & Webb, G. M. 2000 The von Neumann paradox in weak shock reflection. *J. Fluid Mech.* **422**, 193–205.